Original Article

Microsphere incorporation as a strategy to tune the biological performance of bioinks

Journal of Tissue Engineering
Volume 13: 1–18

DOI: 10.1177/20417314221119895
journals.sagepub.com/home/tej
SAGE

Mar Bonany[1,2,3], Laura del-Mazo-Barbara[1,2,3], Montserrat Espanol[1,2,3] and Maria-Pau Ginebra[1,2,3,4]

Abstract

Although alginate is widely used as a matrix in the formulation of cell-laden inks, this polymer often requires laborious processing strategies due to its lack of cell adhesion moieties. The main objective of the present work was to explore the incorporation of microspheres into alginate-based bioinks as a simple and tuneable way to solve the cell adhesion problems, while adding extra biological functionality and improving their mechanical properties. To this end, three types of microspheres with different mineral contents (i.e. gelatine with 0% of hydroxyapatite, gelatine with 25 wt% of hydroxyapatite nanoparticles and 100 wt% of calcium -deficient hydroxyapatite) were synthesised and incorporated into the formulation of cell-laden inks. The results showed that the addition of microspheres generally improved the rheological properties of the ink, favoured cell proliferation and positively affected osteogenic cell differentiation. Furthermore, this differentiation was found to be influenced by the type of microsphere and the ability of the cells to migrate towards them, which was highly dependent on the stiffness of the bioink. In this regard, Ca^{2+} supplementation in the cell culture medium had a pronounced effect on the relaxation of the stiffness of these cell-loaded inks, influencing the overall cell performance. In conclusion, we have developed a powerful and tuneable strategy for the fabrication of alginate-based bioinks with enhanced biological characteristics by incorporating microspheres into the initial ink formulation.

Keywords

Bioink, 3D bioprinting, alginate, microspheres, gelatine, hydroxyapatite

Received: 9 May 2022; accepted: 29 July 2022

Graphical abstract

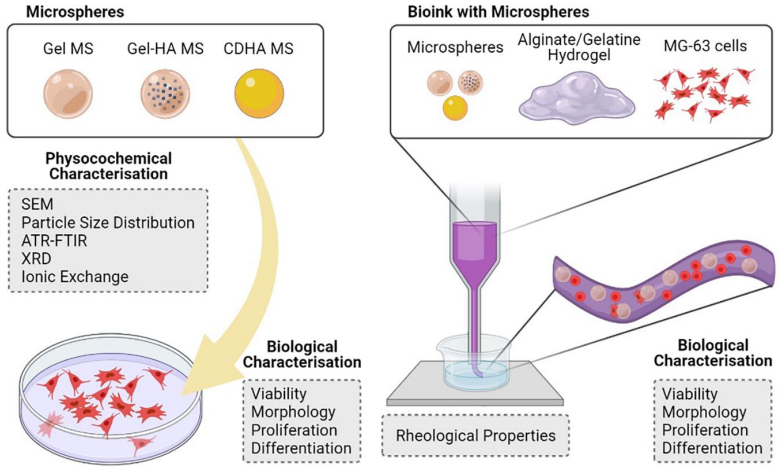

[1]Biomaterials, Biomechanics and Tissue Engineering Group, Department of Materials Science and Engineering, Universitat Politècnica de Catalunya (UPC), Barcelona, Spain
[2]Barcelona Research Centre in Multiscale Science and Engineering, UPC, Barcelona, Spain
[3]Biomedical Engineering Research Center (CREB), UPC, Barcelona, Spain
[4]Institute for Bioengineering of Catalonia (IBEC), Barcelona Institute of Science and Technology, Barcelona, Spain

Corresponding author:
Montserrat Espanol, Universitat Politècnica de Catalunya, Avinguda Eduard Maristany, 16, Barcelona 08019, Spain.
Email: montserrat.espanol@upc.edu

Introduction

In recent years, the tissue engineering field has progressed from two-dimensional (2D) cell culture to 3D models. Indeed, 3D systems are biologically more relevant, as they can reproduce better the physiological environment of the tissues.[1,2] This evolution has been possible thanks to the expansion of additive manufacturing technologies, that permit to develop complex structures using layer by layer deposition. Moreover, they allow to control and tune different features, such as the scaffold architecture or the size and shape of the porosity for the specific application and cell type.[3]

The initial approach concerning 3D models was to generate biocompatible scaffolds that could be further seeded with cells. More recently, 3D bioprinting has advanced these techniques by the loading of cells directly into the ink, creating a promising approach to enhance the regenerative process. Although many advances have been made in the development of extrusion-based bioinks, achieving optimal mechanical and biological requirements simultaneously is challenging.[4] Indeed, low polymer content bioinks, which would be desirable for cell survival and cell migration, may compromise the shape fidelity of the printed struts. In this sense, the ideal cell-laden ink must be mechanically stable and provide high resolution when printed. Regarding the cellular needs, it must be highly biocompatible and allow the proliferation and differentiation of the cells.[5–8]

Hydrogels are the most used materials for the formulation of bioinks, mainly due to their ability to sustain living cells and their adjustable mechanical properties. In particular, alginate is currently one of the most attractive candidates, considering its easy cross-linking capability, which takes place through divalent cation gelation, high availability, low cost and safety (not only for the human body but also for the embedded cells).[9] Nevertheless, its main drawback is the lack of bioactivity, which has led to the implementation of additional processing strategies. One of them is the incorporation of bioactive polymers, such as gelatine, collagen, hyaluronic acid or chitosan among others, to encourage cell adhesion and proliferation in a tissue-specific manner.[10,11] However, due to the complexity of these proteins, it becomes difficult to control the specific signals presented to the cells. The functionalisation of the initial polymer with short cell-adhesive peptides, mainly RGD-based sequences, has been proposed as an alternative way to mimic the ECM and to improve cell attachment and spreading within the bioinks.[12–14] The main drawback of this approach is the need of an additional cross-linking step to bind the bioactive molecule to the alginate,[15,16] which not only lengthens the process but may adversely affect the rheological properties of the final bioink and, in turn, their manipulation and *in vitro* performance.

As an alternative strategy, the combination of alginate with different inorganic materials has been explored, which is especially attractive in the field of bone regeneration as it allow to endow the ink with additional osteogenic cues.[17] The incorporation of bioglass nanoparticles (NPs) capable of delivering biologically active ions such as calcium and silicon in the bioinks has been studied, reporting increased ALP levels and enhanced osteodifferentiation.[18,19] In the same line, the use of hydroxyapatite (HA) particles in gels and bioinks has been proved to increase osteogenic differentiation.[20–22]

Besides the incorporation of nanomaterials, the addition of microspheres (MS) in the formulation of bioinks may be of major interest as they can solve the cell-adhering issues by providing the cells with a surface to attach while improving the mechanical properties of the final constructs. Some studies explored this strategy using polymeric MS.[23–26] Levato et al. added PLA MS into GelMA-based bioinks reporting increased compressive modulus, as well as enhanced cell adhesion and osteogenic differentiation for the condition with pre-seeded MS.[23] Likewise, in the work of Tan et al. the compressive properties of agarose-collagen hydrogels were improved by the incorporation of PLGA MS. Moreover, they demonstrated the viability and proliferation of different cell types pre-seeded on the MS.[24] Abu Awwad et al. explored the delivery of bone therapeutic agents from PLGA MS in a bioprinted system, showing the promotion of osteogenic differentiation of MSC.[25] Despite these findings, studies to date mostly explore the incorporation of organic MS into bioinks. However, in the field of bone regeneration, where the extracellular matrix contains 70 wt% hydroxyapatite, the use of mineral fillers (mostly of nanometre size) has helped to improve bone regeneration.[17,27] We suspected that further advances in the biological performance of the bioinks could be achieved by the addition of inorganic MS larger in size than nanofillers to foster cell adhesion and spreading on the MS surface without the need of using complex ink formulations.[28]

Therefore, we hypothesise that the design of simple, robust and tuneable alginate-based bioinks through the incorporation of microspheres with improved affinity for bone, would be a strong asset to the field of bone bioprinting. MS of three different compositions are analysed, including: (i) gelatine, (ii) hydroxyapatite nanoparticle (HA NP)- containing gelatine; and (iii) calcium-deficient hydroxyapatite (CDHA). The performance of the different MS is tested by direct cell seeding on the MS and also after bioink extrusion of a formulation combining an alginate/gelatine hydrogel with MS and cells. The ability of the cells to colonise the MS in the bioink formulation is further tested using two different degrees of hydrogel cross-linking.

Experimental section

Synthesis of gelatine microspheres

Gelatine microspheres (Gel MS) were prepared by a water-in-oil emulsion. Specifically, a 15 wt% gelatine

(from porcine skin, 250 g Bloom strength, Fluka) solution in bi-distilled water (ddH_2O) was preheated at 50°C. Subsequently, the solution was added dropwise into 50°C preheated 400 ml olive oil with mechanical stirring at 900 rpm to form an emulsion. After 10 min, the mixture was put in an ice bath and stirred for 30 min, prior to the incorporation of cold acetone. The emulsion was left stirring for 1 h before being filtered to collect the synthesised MS. The final powder was rinsed with acetone and left to dry before sieving to the desired particle size (i.e. 40–100 µm). The MS were further cross-linked by immersing them in a cold aqueous solution of 50 mM N-(3-dimethylaminopropyl)-N′-ethylcarbodiimide hydrochloride (EDC, Sigma-Aldrich) and 75 mM N-hydroxysuccinimide (NHS, Sigma-Aldrich) for 1.5 h and thoroughly rinsed with distilled water.

Synthesis of hydroxyapatite-containing gelatine microspheres

For the synthesis of the hydroxyapatite-containing gelatine microspheres (Gel-HA MS), hydroxyapatite nanoparticles (HA NPs) were incorporated into the initial gelatine solution before following the previous protocol. Therefore, HA NPs were produced by wet precipitation method, as described elsewhere.[29] Briefly, 200 mM H_3PO_4 (85 wt% pure, PanReac AppliChem) was added dropwise into a solution of 333 mM $Ca(OH)_2$ (96 wt% pure, Fluka) under constant stirring at 40°C at a rate of 1 ml min^{-1}, according to the equation (1). The supplementation of phosphoric acid was stopped when the pH reached 8 and the product was left stirring for 30 min. Afterwards, stirring was stopped and the suspension was left to mature overnight at room temperature before being rinsed three times with ddH_2O after centrifugation (5430 R, Eppendorf). The final powder was freeze-dried (Cryodos, Telstar).

$$10\ Ca(OH)_2 + 6\ H_3PO_4 \rightarrow Ca_{10}(PO_4)_6(OH)_2 + 18\ H_2O \quad (1)$$

A suspension of 10 wt% HA NPs and 10 wt% sodium citrate (Sigma-Aldrich) was prepared and subsequently sonicated in a high-frequency ultrasound probe sonicator (450D, Branson Digital) using a 3 mm diameter tip at 40% amplitude for 2 min. The dispersion was mixed 1:1 with a 30 wt% gelatine solution and added in the oil as previously described. This resulted in microspheres loaded with 25 wt% of HA (dry weight), which were additionally sieved and cross-linked following the same cross-linking procedure as for the Gel MS.

Synthesis of calcium-deficient hydroxyapatite microspheres

A previously established protocol[30] was adapted for the synthesis of the CDHA MS. The powder phase of the calcium phosphate cement consisted of α-tricalcium phosphate (α-TCP), obtained by sintering a mixture of calcium hydrogen phosphate ($CaHPO_4$, Sigma-Aldrich) and calcium carbonate ($CaCO_3$, Sigma-Aldrich) to a Ca/P ratio of 1.5 in an oven (CRN-58, Hobersal) at 1400°C for 15 h and subsequent quenching in air. The resulting α-TCP was milled in a planetary mill (Pulverisette 6, Fritsch GmbB) to obtain a mean powder-particle size of 2.8 µm,[31] and 2 wt% of precipitated HA (Merck) was added as a seed. In order to obtain the calcium phosphate cement slurry, the seeded α-TCP powder and 1 wt% of sodium citrate were mixed with a 5 wt% gelatine solution in phosphate buffer solution (PBS, Gibco) in a liquid-to-powder ratio of 1.2. This resulted in microspheres with 94 wt% load of mineral content (dry weight).

To synthesise the MS, 3 ml of the ceramic slurry were added drop by drop into 300 ml of olive oil previously heated at 60°C. The emulsion was mechanically stirred (BDC 2002, Heidolph) for 2 h. Afterwards, the MS were separated from the emulsion by the addition of 0.01% Triton X-100 (Sigma-Aldrich) in Ringer's solution (0.9% sodium chloride, PanReac AppliChem). The MS were further washed with acetone and the remaining gelatine cross-linked with EDC/NHS following the previously described protocol. Finally, the powder was immersed in Ringer's solution for a week, to allow the hydrolysis of α-TCP to calcium-deficient HA, according to equation (2). Once the setting was done, the MS were dried and sieved from 40 to 100 µm.

$$3\ Ca_3(PO_4)_2 + H_2O \rightarrow Ca_9(PO_4)_5(HPO_4)(OH) \quad (2)$$

Physicochemical characterisation of the microspheres

The morphological evaluation of the different MS was performed by field emission scanning electron microscopy (FESEM, JSM-7001 F, JEOL) with a previous carbon coating. The size distribution of the MS was assessed through image analysis (FIJI, ImageJ software[32]) of optic microscopy (AE2000, Motic) acquisitions.

Fourier-transform infrared spectroscopy (FTIR, Nicolet 6700, Thermo Scientific) in the attenuated total reflectance (ATR) mode was used to check the presence of the functional groups of apatite and gelatine in the different MS. Data were obtained with a spectral resolution of 4 cm^{-1} and averaging of 64 scans, in the 700 to 2000 cm^{-1} range. Moreover, phase composition of both Gel-HA MS and CDHA MS was determined by X-ray powder diffraction (XRD, D8 Advance, Bruker) using Cu Kα radiation at 40 kV and 40 mA, collecting the data with a step size of 0.02°. The counting time was 2 s per step and the acquisition was done from 20° to 40° 2θ range. The diffractograms were compared to the standard pattern of HA (ICDD PDF 09-0432) for the indexing of the peaks.

In addition, calcium and phosphorus ionic exchanges in cell culture media were measured. 10 mg of MS were put

in contact with 1 ml of Dulbecco's modified eagle medium (DMEM) supplemented with 10% foetal bovine serum (FBS), 20 mM 4-(2-hydroxyethyl)-1-piperazineethanesulfonic acid buffer (HEPES), 2 mM L-glutamine, 50 U ml^{-1} penicillin and 50 µg ml^{-1} streptomycin (all from Gibco), for 4 days. The medium was changed daily and the supernatants were collected, diluted 20-fold in 2 wt% HNO_3 (69 wt% pure, PanReac AppliChem) and analysed by inductively coupled plasma optical emission spectrometry (ICP-OES, 5100, Agilent Technologies). ^{44}Ca and ^{31}P signals were calibrated against a multi-element standard solution (Inorganic Ventures).

Preparation of the bioinks

MG-63 pre-osteoblast cells (ATCC) were cultured in supplemented DMEM in a 95% humidified atmosphere containing 5% CO_2 at 37°C. Previous to cell incorporation in the bioinks, the materials and the powders were sterilised with 70% ethanol or by low-pressure plasma treatment, respectively.

Three formulations were studied, depending on which type of MS was used: Gel, Gel-HA, or CDHA. In addition, a bioink without the addition of MS was used as a control. Moreover, two different cross-linkings were tested, resulting in a total of eight different bioinks. In all the cases, sieved MS (40–100 µm) were used. To facilitate cell assays, all characterisation was performed on extruded filaments.

The bioink formulation was adapted from existing formulations in the literature.[17] More specifically, sodium alginate (PanReac AppliChem) and gelatine were dissolved in DMEM at concentrations of 6 and 8 w/v %, respectively, and mixed in a 1:1 ratio. Cells (2×10^6 cells ml^{-1}) and MS (60 mg ml^{-1}) were incorporated in the inks. The components were thoroughly mixed and homogenised by hand. The mixture was immediately extruded at 30 mm s^{-1} through a 22 Ga nozzle directly to a 150 mM $CaCl_2$ (Sigma-Aldrich) bath, by means of a customised 3D printer (Fundació CIM). Afterwards, the bioinks were rinsed three times with supplemented DMEM and maintained at 37°C and 5% CO_2 atmosphere.

As previously mentioned, two different cross-linking protocols were investigated: (1) a strong cross-linking (sCL) consisting of immersion for 15 min in the $CaCl_2$ bath, followed by maintenance in supplemented DMEM enriched with $CaCl_2$ up to 5 mM and (2) a weak cross-linking (wCL) consisting of immersion for 10 min in the initial $CaCl_2$ bath followed with maintenance in the original supplemented DMEM.

Moreover, discs were prepared for rheological studies. The samples were made by extruding 1 ml of bioink without cells into a $\varnothing = 20$ mm mould and cross-linking them using either wCL or sCL protocols.

Rheological study

The rheological properties of the four bioinks formulations without cells were analysed. The measurements were carried out on a rotational rheometer (Discovery HR-2, TA Instrument), using a rough parallel plate geometry ($\varnothing = 20$ mm) with a gap of 1 mm (10 times the size of the MS). First, an oscillatory amplitude sweep was performed from 10% to 1000% at a constant frequency of 1 Hz to analyse the viscoelasticity. The second test was a 3-interval thixotropy test (3-ITT) to study the thixotropy and the shape-retention ability of the bioinks. Precisely, it consisted of three consecutive oscillatory intervals, all of them at a constant frequency of 1 Hz: (1) a low strain within the linear viscosity region (LVR) of the previous amplitude sweeps (i.e. 10%) for 1 min to simulate the rest condition of the bioink before being extruded, (2) a high strain, above the fluid point of the amplitude sweep (i.e. when $G' = G''$, 700%) for 30 s to mimic the extrusion process and (3) the conditions of the first interval to simulate the rest condition of the bioink just immediately after being extruded. The data of the third interval was acquired using a fast sampling mode, in contrast to the normal acquisition mode used in the other intervals.

Additionally, the two CL used in the present work were compared placing the different hydrogels -shaped as discs- between the rheometer plates. The rheological analysis was performed at the same rotational rheometer using a rough parallel plate geometry ($\varnothing = 20$ mm) with a gap of 3 mm. Specifically, the test consisted of a short oscillatory step with a strain of 10% (within the LVR of the bioinks) and a constant frequency of 1 Hz for 2 min to mimic the rest conditions of the bioinks just immediately after extrusion. Each sample was analysed at 0, 7 and 14 days.

Direct cell culture on the microspheres

The behaviour of MG-63 cells in direct contact with the different MS was examined and compared to the biological results of the bioink. To do so, 48-well plates were treated with 1 wt% albumin in PBS to prevent cell adhesion. 10 mg of MS were added to each well and MG-63 cells were seeded on top at a concentration of 50,000 cells ml^{-1}. A control sample with no MS was also included in the study. The biological performance was examined in terms of cell viability, cell proliferation, cell morphology and gene expression, using the following protocols.

Cell viability analysis

The migration and the viability of the MG-63 either cultured directly on the MS or inside the bioinks were assessed by live/dead (L/D) staining at different time points (i.e. 0, 3, 7, 14 and 21 days). Specifically, 3 µM calcein AM (Santa

Table 1. Primers' sequences used for RT-qPCR.

Gene	Primers' sequences (Fw = forward; Rv = reverse)
Glyceraldehyde 3-phosphate dehydrogenase (GAPDH)	Fw: 5′-TTGCCATCAATGACCCCTTCA-3′ Rv: 5′-CGCCCCACTTGATTTTGGA-3′
Alkaline phosphatase (ALP)	Fw: 5′-ATCTTTGGTCTGGCTCCCATG-3′ Rv: 5′-TTTCCCGTTCACCGTCCAC-3′
Collagen type I (Col. I)	Fw: 5′-AGGTCCCCCTGGAAAGAA-3′ Rv: 5′-AATCCTCGAGCACCCTGA-3′
Runt-related transcription factor 2 (RUNX2)	Fw: 5′-AAATGCCTCCGCTGTTATGAA-3′ Rv: 5′-GCTCCGGCCCACAAATCT-3′
Osterix (OSX)	Fw: 5′-TGCTTGAGGAGGAAGTTCAC-3′ Rv: 5′-AGGTCACTGCCCACAGAGTA-3′
Osteopontin (OPN)	Fw: 5′-AGCTGGATGACCAGAGTGCT-3′ Rv: 5′-TGAAATTCATGGCTGTGGAA-3′
Osteocalcin (OCN)	Fw: 5′-ATGAGAGCCCTCACACTCCT-3′ Rv: 5′-CTTGGACACAAAGGCTGCAC-3′

Cruz Biotechnology) and 1.5 µM propidium iodide (PI, Sigma-Aldrich) were supplemented to the cells into fresh media as indicators of live and dead cells, respectively. The stained cells were imaged under a laser confocal scanning microscope (LSM 800, Zeiss). In addition, the images of the bioinks obtained at day 0 were used to quantify the cell viability after the extrusion using ImageJ software.

Cell proliferation and cell morphology evaluation

Cell proliferation either on the MS or inside the hydrogels was evaluated at 0, 3, 7, 14 and 21 days with Presto Blue (Invitrogen) assay, following the manufacturer's instructions and measuring the fluorescence in a microplate reader (540 nm excitation/590 nm emission wavelengths). Afterwards, the samples were rinsed with PBS to remove the staining and fresh cell culture media was added.

The evaluation of the cell morphology and the cell adhesion to the MS was done at days 3, 7 and 14 for the cells cultured with the MS, and after 21 and 14 days in culture for sCL and wCL bioinks, respectively. The specimens were rinsed with PBS and subsequently fixed with 4 wt% paraformaldehyde solution (PFA, EMS) for 20 min at room temperature. The cells were permeabilised through incubation with 0.05% Triton X-100 in PBS for 15 min before staining them with Alexa Fluor 546 phalloidin (1:400, Invitrogen) in 0.05% Triton X-100 for 1 h. For nuclei staining, the samples were put in contact with 4′,6-diamidino-2-phenylindole (DAPI, 1:1000, Sigma-Aldrich) for 2 min. All steps were followed by rinsing with 0.15% glycine solution (Sigma-Aldrich) in PBS. Finally, the samples were visualised with the confocal LSM.

In addition, the cell adhesion and spreading was checked by SEM (Phenom XL, PhenomWorld) in the wCL Gel MS-containing bioink. The samples cultured for 14 days were fixed with 2.5% glutaraldehyde solution and dehydrated in an increasing series of ethanol solutions. Afterwards, they were allowed to dry at 37°C and the surface of the samples was coated with a carbon- evaporated layer using EMITECH K950X. Images were taken at an acceleration voltage of 10 kV.

Gene expression assessment

The cell differentiation to osteoblastic phenotype was assessed by measuring the gene expression of osteogenic markers through real-time quantitative polymerase chain reaction (RT-qPCR). Prior to the mRNA extraction with RNeasy Mini Kit (Qiagen), the bioinks were incubated with alginate-dissolving buffer (55 mM sodium citrate, 30 mM EDTA, 150 mM NaCl, pH = 6.8) for 10 min at 37°, and the alginate was eliminated by centrifuging 10 min at 300 *g*. The RNA obtained was quantified spectrophotometrically with Take3 micro-volume plate (BioTek Instruments) and reverse transcription was performed using QuantiTect Reverse Transcription Kit (Qiagen). cDNA was amplified with the QuantiFast SYBR Green RT-PCR Kit (Qiagen) in a Mic qPCR Cycler (Biomolecular Systems), using specific primers listed in Table 1. In all runs, melt curve analysis was done to ensure the specificity of the primers. Moreover, a negative control was run in parallel to verify the absence of contamination. Relative gene expression levels were evaluated using the $2^{-\Delta\Delta Ct}$ method and GAPDH was used as housekeeping gene. Data were normalised to the control at day 3 and 7 for the culture onto the MS and in the bioinks, respectively.

Statistical analysis

All data are presented as mean ± standard deviation, except for the viability and proliferation outcomes, where mean ± standard error of the mean is reported. The distribution of the data was checked with Shapiro-Wilk test.

Significant differences between samples were determined using ANOVA followed by Tukey's posthoc test or Kruskal-Wallis test for normally and non-normally distributed data, respectively. Significance level was set for $p < 0.05$. Statistical analysis was performed using SPSS software.

Results

Physicochemical characterisation of the microspheres

The morphology and microstructure of the different MS observed by SEM are depicted in Figure 1(a). All the conditions, that is Gel MS, Gel-HA MS and CDHA MS, showed a high degree of sphericity and the diameter size was shown to be in the range of 40–100 μm, as expected from the sieving step. Moreover, needle-shaped HA NPs were observed, embedded in a gelatine matrix, in the Gel-HA MS when the backscattering detector was used. The microstructure of the CDHA MS resembled spherulitic aggregates consisting of an entangled network of nanometric plate-like crystals, formed during the hydrolysis of α-TCP to CDHA.

Image analysis was performed to determine the size distribution of the MS. As observed in Figure 1(b), all of them presented a monomodal normal particle size distribution. The average size diameter of the three types of MS was similar in dry conditions, being Gel MS the ones with the largest size, with a mean value of 82 ± 16 μm. On the other hand, Gel-HA MS and CDHA MS showed a mean size of 73 ± 17 and 55 ± 15 μm, respectively. Although gelatine was chemically cross-linked, the MS increased their volume in contact with an aqueous solution due to swelling. Thus, the particle size increased to 106 ± 30 μm for Gel MS and 123 ± 32 μm for the Gel-HA MS. An almost negligible volume gain was observed for the wet CDHA microspheres, reaching an average diameter of 67 ± 17 μm, which was consistent with their mostly inorganic nature.

Figure 1(c) compiles experimental ATR−FTIR patterns of both gelatine and HA NPs, together with the spectra obtained for the different synthesised MS. The gelatine spectrum presented the amide I band corresponding to the C=O stretching at $\approx 1650\,cm^{-1}$, the amide II bands at $\approx 1550\,cm^{-1}$ and $\approx 1450\,cm^{-1}$ of NH and CH_2 bending, respectively, and the amide III band in the range 1250–650 cm^{-1}, with the NH bending shown at $\approx 1240\,cm^{-1}$.[33] On the other hand, the HA NPs spectrum exhibited the typical PO_4^{3-} absorption bands at 960 and 1030–1100 cm^{-1}, corresponding to the symmetric stretching (ν_1) and asymmetric stretching (ν_3) vibrational modes of the P-O bond, respectively.[34,35] Moreover, the presence of additional bands was detected at 870, 1414 and 1470 cm^{-1}, representative of the out-of-plane bend vibration (ν_2) and asymmetric stretch vibration (ν_3) of CO_3^{2-}[36,37]. These findings suggested B-type carbonation of apatite, probably caused by the dissolution of CO_2 during the synthesis of the HA NPs.[29] In addition, the small band appearing at 870 cm^{-1} in the CDHA accounts for the presence of HPO_4^{2-}, which is typical in CDHA, as observed in equation (2).[38] All MS spectra matched with these patterns and the relative intensity of the characteristic bands of gelatine and HA found in each condition was consistent with their composition (i.e. Gel MS only contained gelatine, Gel-HA MS were composed of 75 wt% gelatine and 25 wt% HA, and CDHA MS were made of 6 wt% gelatine and 94 wt% CDHA). No other unidentified bands were detected, which indicates the absence of unreacted compounds within the limits of detection of the technique (i.e. EDC, NHS and sodium citrate).

The XRD analysis (Figure 1(d)) revealed that the inorganic phase in both Gel-HA MS and CDHA MS were phase pure with no other peaks than those corresponding to the apatite phase. In addition, in both cases, broad peaks were observed, which accounts for the low-crystallinity of the resulting apatitic product, compatible with its nanometric nature. In the case of CDHA MS, it was demonstrated that the end-product of the hydrolysis of α-TCP was CDHA and that the presence of gelatine did not hinder the reaction.

ICP-OES results depicted in Figure 1(e) revealed that Ca^{2+} and P_i concentrations in the DMEM medium were 2.01 ± 0.05 and 1.30 ± 0.02 mM, respectively, and remained stable during the whole experiment. A small alteration of both ion levels was observed when Gel MS were immersed in DMEM, with around 13% lower values throughout the study. In contrast, a more pronounced decrease of Ca^{2+} and P_i concentration was found when Gel-HA MS and CDHA MS were immersed in the culture medium. Both uptook Ca^{2+} ions from the medium, reaching concentrations of 1.11 and 1.28 mM after 4 days in culture, respectively. Following the same trend, P_i levels in Gel-HA MS and CDHA MS were considerably reduced all along the study. Indeed, P_i levels in Gel-HA MS were the lowest at all the time points, reaching a reduction of up to 50% at day 4.

Rheology and shape fidelity of the bioinks

Rheological studies of the four different bioink formulations were performed without the addition of cells. The bioink formulation consisted of an alginate-gelatine hydrogel mixed with the different MS (Gel MS, Gel-HA MS and CDHA MS). A hydrogel without MS was included as a control.

The outcome of the oscillatory amplitude sweep (Figure 2(a)) showed a viscoelastic behaviour of the four bioinks, as evidenced by a LVR of solid-like behaviour ($G' > G''$ and constant moduli) at low and medium strains, followed by a transition to liquid behaviour at high strains, where G'' became higher than G'. The damping factor (G''/G' at

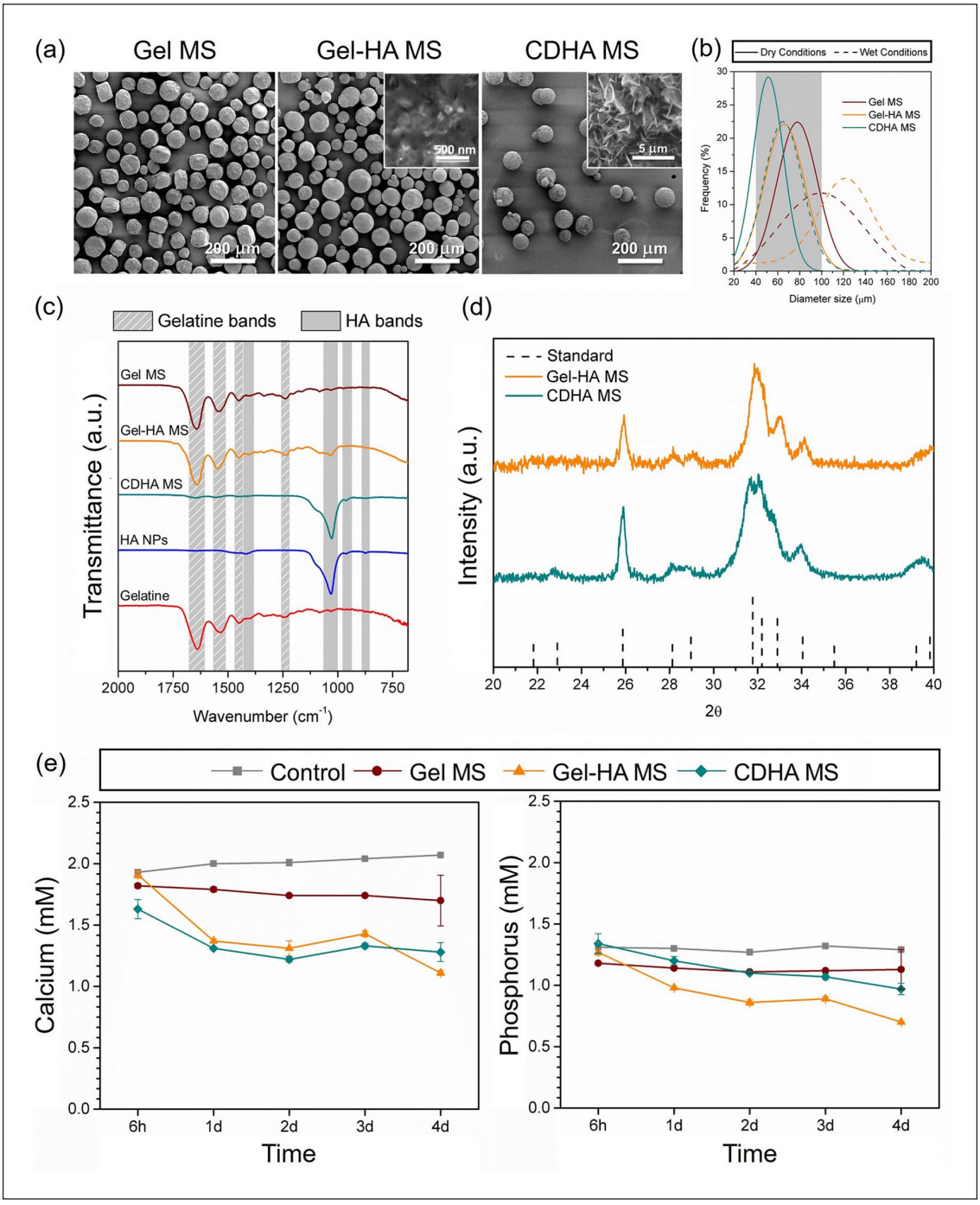

Figure 1. Physicochemical characterisation of Gel MS, Gel-HA MS and CDHA MS. (a) SEM images of the MS and high-magnification in the insets showing their surface. (b) Size distribution of the different MS, in both dry and wet conditions. The MS were sieved from 40 to 100 µm before the measurement, the grey area represents the sieving applied. (c) ATR-FTIR spectra of the synthesised MS, along with the spectra of the commercial gelatine and the synthesised HA NPs. Stripped and shaded regions correspond to the characteristic bands of gelatine and HA NPs, respectively. (d) X-ray diffraction patterns of Gel-HA MS and CDHA MS. (e) Calcium and phosphorus concentration of the cell culture media in contact with the various MS for 4 days, determined by ICP-OES.

rest conditions) was calculated and compiled in Table 2. Interestingly, the damping factor obtained for Gel MS and CDHA MS bioinks was similar to the control. In contrast, Gel-HA MS bioink presented a larger distance between both moduli, with a damping factor of 0.33, indicating a higher elastic behaviour than the other conditions.

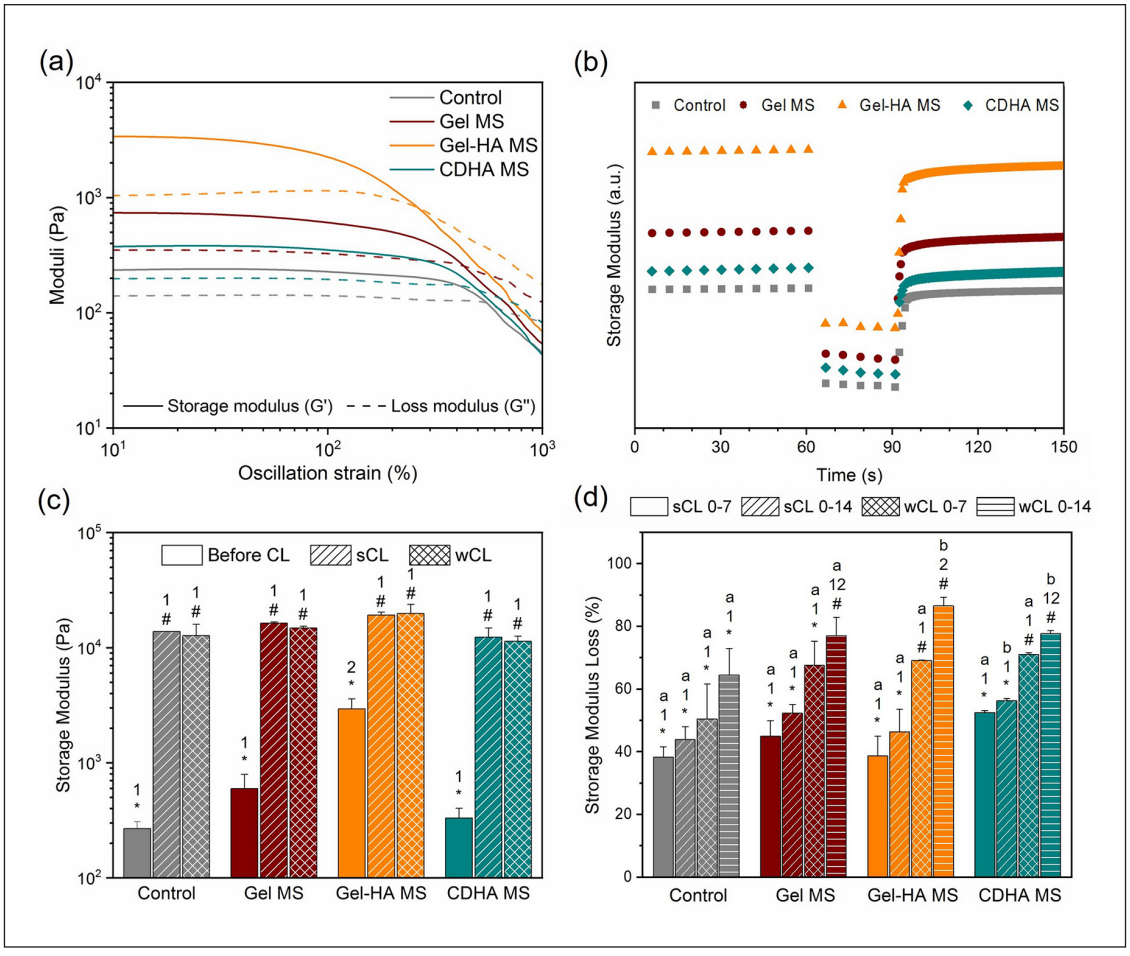

Figure 2. Rheological properties of the synthesised bioinks. (a) Oscillatory amplitude sweep results showing the G′ and G″ evolution over strain. (b) G′ recovery of the bioinks after being put under a high strain to mimic the extrusion process. (c) G′ of each condition after being cross-linked for 15 or 10 min corresponding to the sCL and wCL protocols, compared to the non-cross-linked samples. (d) G′ loss of the two cross-linkings studied after 7 and 14 days in culture. Different letters indicate statistically significant differences between time points in the same condition, different numbers indicate statistically significant differences between conditions, and different symbols indicate statistically significant differences between cross-linkings ($p < 0.05$).

Table 2. Data obtained from the oscillatory amplitude sweep assay.

	G'_{eq} (Pa)	G''_{eq} (Pa)	Damping factor	Yield stress (Pa)	Flow stress (Pa)
Control	268 ± 40	151 ± 13	0.5634	281 ± 30	989 ± 53
Gel MS	598 ± 197	308 ± 59	0.5150	310 ± 04	1409 ± 200
Gel-HA MS	2937 ± 645	958 ± 115	0.3261	917 ± 80	2926 ± 166
CDHA MS	332 ± 71	185 ± 21	0.5572	314 ± 10	1025 ± 128

Furthermore, the addition of Gel MS increased the equivalent elastic modulus (G'_{eq}, storage modulus at rest conditions) of the bioink from 268 ± 40 Pa to 598 ± 197 Pa, whereas with the incorporation of Gel-HA MS, this effect was significantly higher, reaching a G'_{eq} of 2937 ± 645 Pa. In contrast, the addition of CDHA MS resulted in low G'_{eq} increase of up to 332 ± 71 Pa. As a consequence, the yield stress (the end of the LVR, when the G′ starts to decrease) was much higher in the Gel-HA MS (917 ± 80 Pa) than in the other bioinks, which presented similar values: 281 ± 30, 310 ± 4, and 314 ± 10 Pa for control, Gel MS and CDHA MS, respectively. Finally, the flow stress, that is, the beginning of the flow region (when $G' = G''$), was affected in an analogous way to the G'_{eq}, but with smaller increments. In particular, the control condition presented flow stress of 989 ± 53 Pa, Gel MS of 1409 ± 200 Pa, Gel-HA MS of 2926 ± 166 Pa and CDHA MS of 1025 ± 128 Pa.

The 3-ITT test evidenced a G′ recovery of 91% for the control, 84% for Gel MS, 73% for Gel-HA MS and 88% for CDHA MS just 5 s after being sheared at a high strain (Figure 2(b)). Moreover, the recovery after 30 s was almost complete for the control bioink (97%), Gel MS (92%) and CDHA MS (96%). On the other hand, Gel-HA MS bioink recovered 81% of its initial G′.

To compare the effect of the cross-linking degree, wCL (weakly cross-linked) and sCL (strongly cross-linked) discs were prepared for each condition and cross-linked for 10 and 15 min, respectively. As seen in Figure 2(c), the cross-linking process was crucial for achieving self-supporting bioinks, as the storage modulus increased up to 10,000 Pa. Moreover, the final G′ was found to be similar in all the cases, irrespective of the initial G'_{eq} differences among them. On the other hand, the progressive degradation of the cross-linked hydrogels during the culture was evident in all the conditions, as shown in Figure 2(d). The wCL discs containing MS lost around 70% of their G′ after 7 days of culture, while the loss in the control disc was slightly lower, of around 50%. This cross-linking reduction along the time led to a final G′ decrease of 80% for the MS-containing discs and 65% for the control discs after 14 days of incubation. In the case of sCL samples, the G′ loss was around 40%–50% in all the conditions at day 7, increasing an additional 5% loss at day 14 for all the samples. These findings demonstrated that the Ca^{2+} supplementation in the cell culture media was key for the preservation of the cross-linking of the hydrogels.

Cell cultures on the microspheres

The following sections address the biological response of the cells when seeded on the microspheres and within the bioinks. Regarding the behaviour of the cells seeded on the microspheres, cell viability, proliferation, morphology and gene expression were examined. The results after 1 day of cell culture showed that the initial cell adhesion to all MS types was similar, as observed in Figure 3(a) and quantified in Figure 3(c). After 3 days of cell culture, cell proliferation was promoted especially on Gel MS and Gel-HA MS. Nevertheless, cell counts were comparable between conditions at day 14 (≈3-fold of the initially seeded cells), confirming a proper cell growth in all the samples throughout the study, with a similar proliferation rate over the study for all the MS. Regarding the distribution of the cells on the MS, L/D images revealed that cells adhered to all three types of MS and had the ability to proliferate and fully colonise them. However, a non-negligible number of dead cells were detected in CDHA MS samples at day 7 and 14.

The actin fibres and nuclei stainings in Figure 3(b) helped to certify the cell adhesion on the MS of all natures, as well as their organisation in the samples. Indeed, in all the conditions cells tended to attach, spread and multiply on the surface and in-between the MS. Furthermore, the expression of osteogenic genes was examined and is summarised in Figure 3(d). In general, CDHA MS presented the most osteoinductive properties among the different MS. When compared to the control, cells on CDHA MS exhibited a 4.5-fold expression of ALP at day 3, a 2 or 2.5-fold expression of Col. I at all the time points, a 4-fold expression of OPN at day 7, and a general 2-fold expression of OCN. Moreover, Gel-HA MS also upregulated the expression of Col. I at days 3 and 14, of OPN at day 14 and of OCN at day 7 of culture, all of them with a 1.5-fold relative to the control. The contribution of the HA NPs was observed comparing the results of Gel-HA MS and Gel MS in terms of ALP expression at day 3 and the expression of OPN and OCN at 14 and 7 days, respectively, although not all the differences were statistically significant. Interestingly, RUNX2 had an important overexpression of 4-fold and 5-fold at day 14 for Gel-HA MS and CDHA MS, respectively, yet the expression in Gel MS was the highest with a 7-fold change to the control.

Cell viability and cell migration in the bioinks

In order to study the performance of the cells in the bioinks, four different formulations were prepared by mixing the alginate, the gelatine and each type of MS with the cells. A control bioink without the incorporation of MS was also included. The extrusion was done through a 22 Ga nozzle directly into a $CaCl_2$ bath, as described in the experimental section. In addition, two different cross-linking protocols were investigated (i.e. wCL and sCL). The sCL allowed to study the final constructs up to 21 days of cell culture, while the wCL bioinks lost stability after 14 days in culture.

The visualisation of the cells embedded in the bioinks was done by confocal microscopy. Representative live/dead (L/D) images in Figure 4(a) and (b) proved that ⩾90% of the cells were viable (green fluorescent cells) and only a small number of dead cells (red fluorescent ones) were observed at 3, 7, 14 and 21 days of culture for all the conditions. In contrast, the L/D ratios immediately after the extrusion (i.e. at day 0) were slightly lower, especially for the bioinks containing Gel-HA MS and CDHA MS, independently of the cross-linking protocol applied. Therefore, the viability at day 0 was quantified for the two initial cross-linking times and compared among the four bioinks. Figure 4(c) shows that in general, the differences between the cross-linkings were minimal, demonstrating that their effects on cells at the initial time point were similar. Moreover, it was observed that the control condition presented the highest cell viability (93.0% ± 0.4), followed by the Gel MS bioink with 90.8% ± 0.9 of the cells alive. A significant decrease in the viability of the cells was found in the other two conditions, indicating that the incorporation of apatite-containing MS reduced the cell survival rate at earlier time points. Indeed, Gel-HA MS

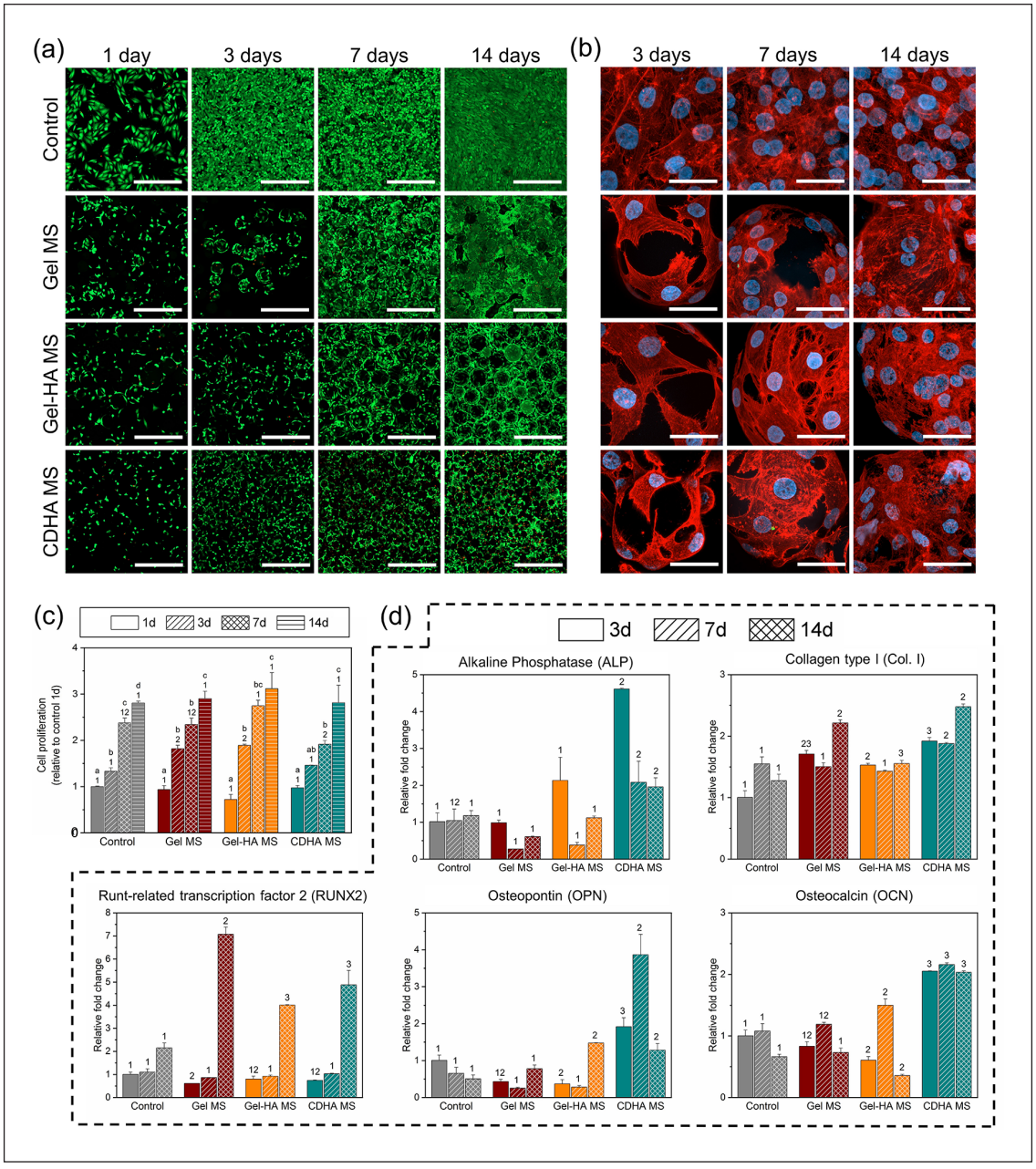

Figure 3. Behaviour of MG-63 cells cultured on the different MS. (a) Live/dead staining images at day 1, 3, 7 and 14. Live cells stained in green and dead cells in red. Scalebar represents 500 µm. (b) Cell morphology pictures at 3, 7 and 14 days of culture. Cell nuclei in blue and actin fibres in red. Scalebar represents 40 µm. (c) Cell proliferation measured through resazurin-based method. (d) Gene expression of osteogenic markers for the cells seeded in the MS at day 3, 7 and 14. Control samples at day 3 were used as a reference to determine the fold changes. Different letters indicate statistically significant differences between time points in the same condition and different numbers indicate statistically significant differences between conditions at each time point ($p < 0.05$).

exhibited cell mortality of 21.3% ± 1.5, similar to that of CDHA MS bioinks with 18.4% ± 1.2 of dead cells. In spite of this, the initial viability rates for all the bioinks were sufficient for the cells to survive and proliferate, indicating a suitable performance for all the conditions. Figure S1 in the Supplemental Information provides fluorescence confocal images of the printed bioinks to demonstrate the homogeneous distribution of MS in all formulations.

With regards to the evolution of the cells in the bioinks, it was observed that initially MG-63 cells were embedded in the alginate matrix. We believe that after several days of culture, cells close to the MS began to migrate, adhere and proliferate to the Gel MS and Gel-HA MS, as can be appreciated in the insets of Figure 4(a) and (b). The time needed for this process highly depended on the cross-linking applied: in the bioinks with sCL the migration started at

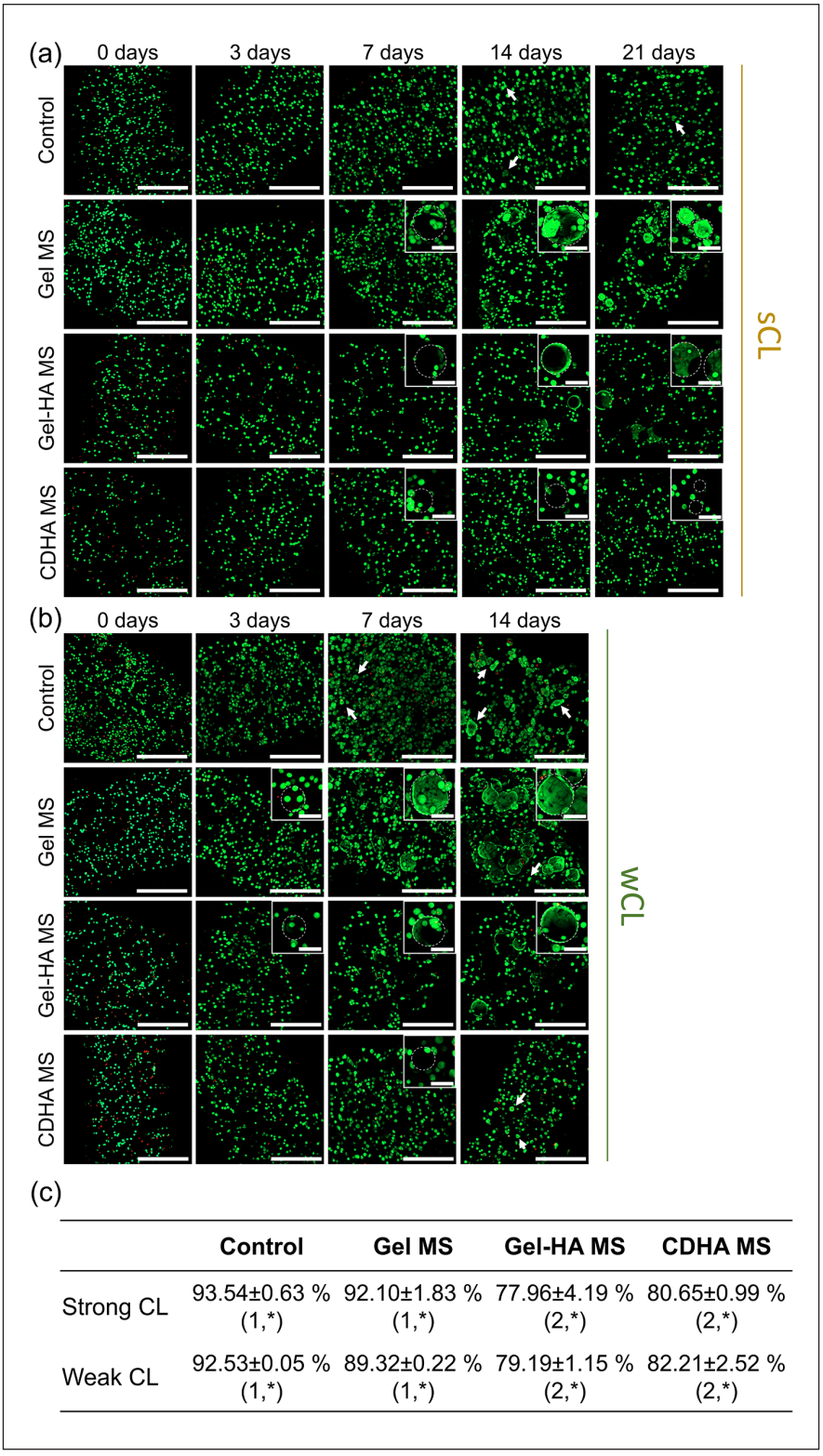

(c)

	Control	Gel MS	Gel-HA MS	CDHA MS
Strong CL	93.54±0.63 % (1,*)	92.10±1.83 % (1,*)	77.96±4.19 % (2,*)	80.65±0.99 % (2,*)
Weak CL	92.53±0.05 % (1,*)	89.32±0.22 % (1,*)	79.19±1.15 % (2,*)	82.21±2.52 % (2,*)

Figure 4. Evolution of MG-63 cell viability in the different bioinks. Live/dead images of the bioinks with sCL (a) and wCL (b) at 0, 3, 7, 14 and 21 days of culture. Live cells stained in green and dead cells in red. Insets show magnification of cells attached to the different MS. Dashed circles indicate MS, and arrows cell clusters forming spheroids. Scalebars represent 500 µm for the full images and 100 µm for the insets. (c) Quantification of the cell viability at day 0, immediately after the bioinks extrusion. Different numbers indicate statistically significant differences between conditions for each CL and different symbols indicate statistically significant differences between cross-linkings within the same condition ($p < 0.05$).

day 7 (Figure 4(a)), while the bioinks with wCL exhibited cell migration and attachment to the MS earlier, at day 3 (Figure 4(b)). Although to a lesser extent, the confocal images also proved that these phenomena occurred in the CDHA MS bioinks.

It is worth noting that at the latest time points evaluated (i.e. 14 days for wCL and 21 days for sCL), the cells that remained unattached to the MS increased their size in some of the conditions (marked with arrows), especially in the control and Gel MS bioinks in the case of the wCL bioink (Figure 4(b)). This observation suggested the formation of small cell spheroids as a consequence of cell growth, which will be further analysed in the next section.

Cell proliferation and cell morphology in the bioinks

Cell proliferation in the bioinks was evaluated through Presto Blue assay at 0, 3, 7, 14, and 21 days (Figure 5(a) and (b)). The results confirmed the proliferation of MG-63 in all conditions. In the case of sCL bioinks, the cell number in all the MS-containing bioinks remained unaltered for the first week and registered a 3-fold increase from day 7 to day 14, reaching a plateau that lasted until day 21. In contrast, the cell number in the control bioink exhibited a constant growth throughout the cell culture, up to 5-fold increase at day 21. Regarding the wCL bioinks, similar proliferation rates were found also for all the conditions at each time point. Cell number rose sharply from day 0 to day 3 in all the bioinks and afterwards, cell growth essentially stopped at a 4-fold cell number for MS-containing bioinks and 3.5-fold value for the control samples. In general, the results showed that all MS-loaded bioinks supported cell proliferation, reaching a plateau of cell population earlier or later depending on the degree of cross-linking. The stronger the cross-linking, the longer it took for the cells to start proliferating and to reach the final plateau.

Figure 5(c) and (d) display the morphology of the cells inside the different bioinks at the last incubation time point, investigated using phalloidin and DAPI to stain the actin filaments and the nuclei, respectively. Overall, proper attachment and spreading were observed for the cells adhered to the MS in the Gel MS and Gel-HA MS samples (top rows of Figure 5(c) and (d)). In contrast, CDHA MS bioink was not able to promote cell migration and attachment to the MS. In general, the cells that were not adhered to the MS presented rounded morphologies, typical of alginate-based bioinks. It was noticeable their ability to cluster and form cell spheroids for all the conditions, as evidenced in the bottom rows of Figure 5(c) and (d). Bigger spheroids were found in the pristine bioink, compared to the MS-containing formulations. Moreover, although cell morphology was comparable in the two CL conditions, it was observed that the wCL allowed the formation of larger cell colonies, as evidenced by the number of nuclei in each spheroid (bottom row of Figure 5(c) vs. bottom row of Figure 5(d)), especially seen in the control specimens. All these findings are in agreement with the L/D results of the previous section.

Additionally, SEM images were taken for the wCL Gel MS bioink (Figure 5(e)). The prior dehydration of the sample resulted in the exposure of the embedded MS through the alginate network, showing the cells well attached and spread on the MS, in agreement with the confocal microscopy results.

Gene expression of the cells in the bioinks

Since the wCL bioinks promoted a faster cell response compared to the sCL condition, wCL specimens were chosen for the gene expression analysis of osteogenic markers. Overall, the MS-containing bioinks presented an overexpression of all the osteogenic genes compared to the control sample, irrespective of their nature. Analysing the results in more detail, they indicated that Gel MS significantly upregulated the expression of ALP, RUNX2, OSX and OPN at day 7 but most notably at 14 days of culture, as shown in Figure 6. In the case of Gel-HA MS, Col. I and OCN genes presented the highest expression for the two studied time points, with a ≈4-fold (at day 7) and ≈6-fold (at day 14) increase of Col. I gene with respect to the control, with statistically significant differences. In contrast, CDHA MS showed low expression of these genes, although presenting an overexpression of OSX at 14 days.

Discussion

The development of bioinks requires a compromise between the improvement of their biological performance and their mechanical properties. Alginate-based bioinks are typically chemically modified to provide cell adhesive moieties to improve the behaviour of the embedded cells. However, their rheological properties can be detrimentally altered by these modifications. In the search for the optimal bioink, we propose the incorporation of microspheres with different bone-related functionalities to an alginate-based bioink to enhance both cell attachment and differentiation while improving their mechanical performance. The initial hydrogel composition consisted of a mixture of alginate (6 wt%) and gelatine (8 wt%). While alginate supported cell viability, kept the MS embedded in the alginate matrix due to its ability to gel in the presence of Ca^{2+} ions, and provided mechanical stability to the construct; the role of gelatine was to improve the rheological properties of the ink and to provide a protective environment for the cells during extrusion and in the initial hours of culture. Subsequently, gelatine was expected to gradually diffuse out of the inks during cell culture, as no gelatine cross-linking treatment was applied.

In this study, microspheres of three different compositions were successfully synthesised. Gelatine MS (Gel

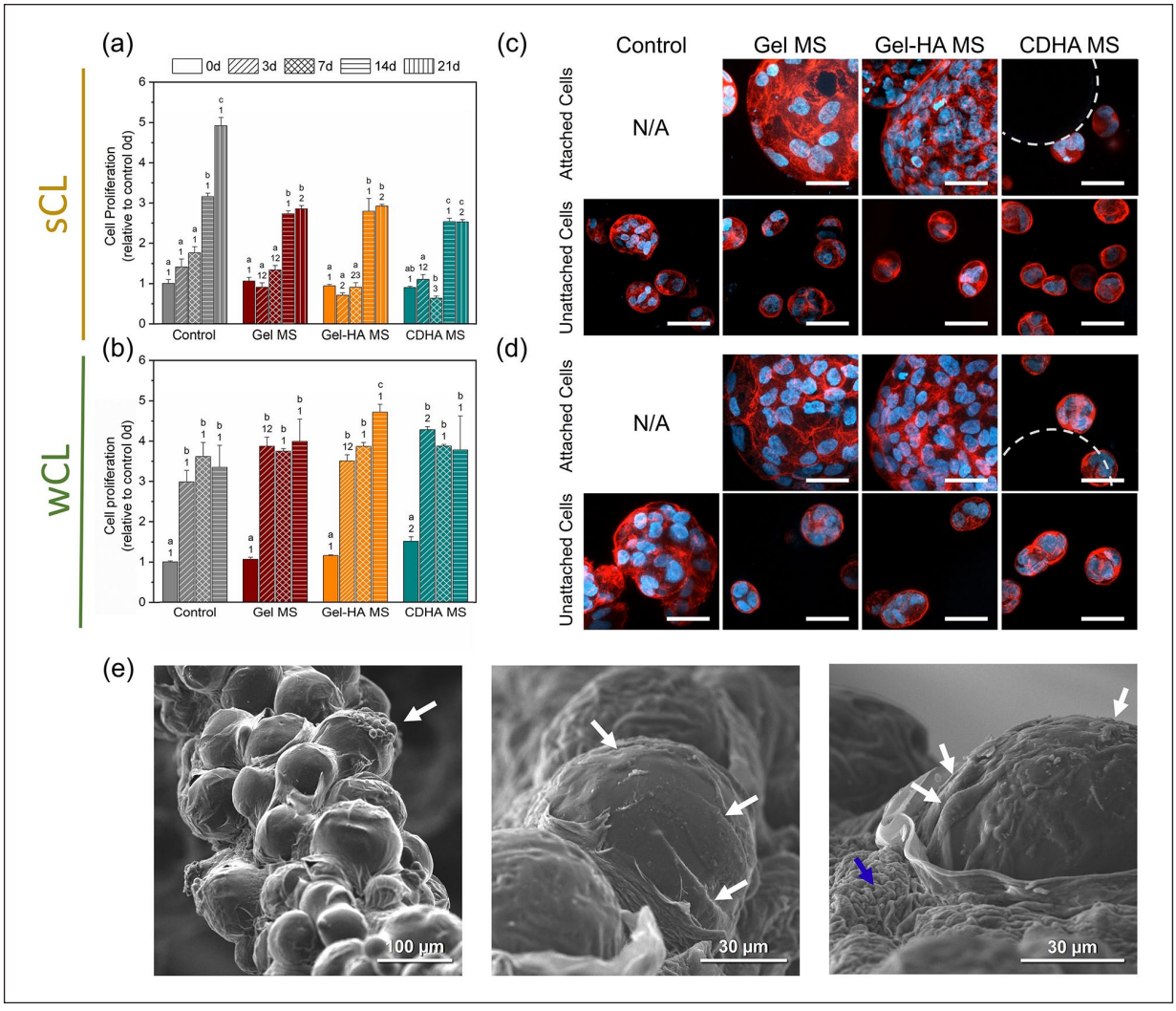

Figure 5. Cell behaviour in the developed bioinks. (a) Cell proliferation results of the sCL samples and (b) of the wCL condition along the study. Different letters indicate statistically significant differences between time points in the same condition and different numbers indicate statistically significant differences between conditions at each time point ($p < 0.05$). (c) Cell morphology in the sCL bioinks at day 21 and (d) in the wCL bioinks at day 14, observed by fluorescence confocal microscopy. Top rows show cells attached to the MS inside the bioinks, bottom rows exhibit unattached cells suspended within the cell-laden ink. Nuclei in blue and actin fibres in red. Dashed circles indicate CDHA MS. Scalebars denote 50 µm. (e) SEM images of the wCL Gel MS bioink. White arrows indicate cells attached and spread on the MS, blue arrow indicates alginate.

MS) were chosen for its biocompatibility,[39] while calcium phosphate containing-MS were selected as a possible strategy to enhance the osteogenic or osteoinductive properties of the bioinks.[31,40,41] Their microstructure and chemical composition was verified by SEM, FTIR and XRD (Figure 1(a), (c) and (d)). The size of the cross-linked gelatine-containing MS (i.e. Gel MS and Gel-HA MS) sieved from 40 to 100 µm experienced substantial swelling in cell culture medium due to hydration of their gelatine phase (Figure 1(b)). The Gel-HA MS presented the most pronounced swelling, which can be explained by the partial blocking of the carboxylic groups involved in the cross-linking of the gelatin chains by the Ca^{2+} of the NPs. This phenomenon could prevent the cross-linking between the hydrogel chains, causing their swelling.[42] Importantly, the bioactive nature of the apatite containing-MS (i.e. Gel-HA MS and CDHA MS), explained by the inherent reactivity of the apatitic nanocrystals,[43] was indirectly proved by the substantial changes in the calcium and phosphorus concentrations in the cell culture media when the microspheres were directly exposed to it (Figure 1(e)).

Understanding the rheological properties of the bioinks is fundamental to predict their printability. In this sense, all the bioinks developed in the present work presented a viscoelastic behaviour, as observed in Figure 2(a), which is required in direct ink writing techniques, since the material must be extrudable at high shear rates while assuring a perfect deposition and shape fidelity.[44] Moreover, it was found that the

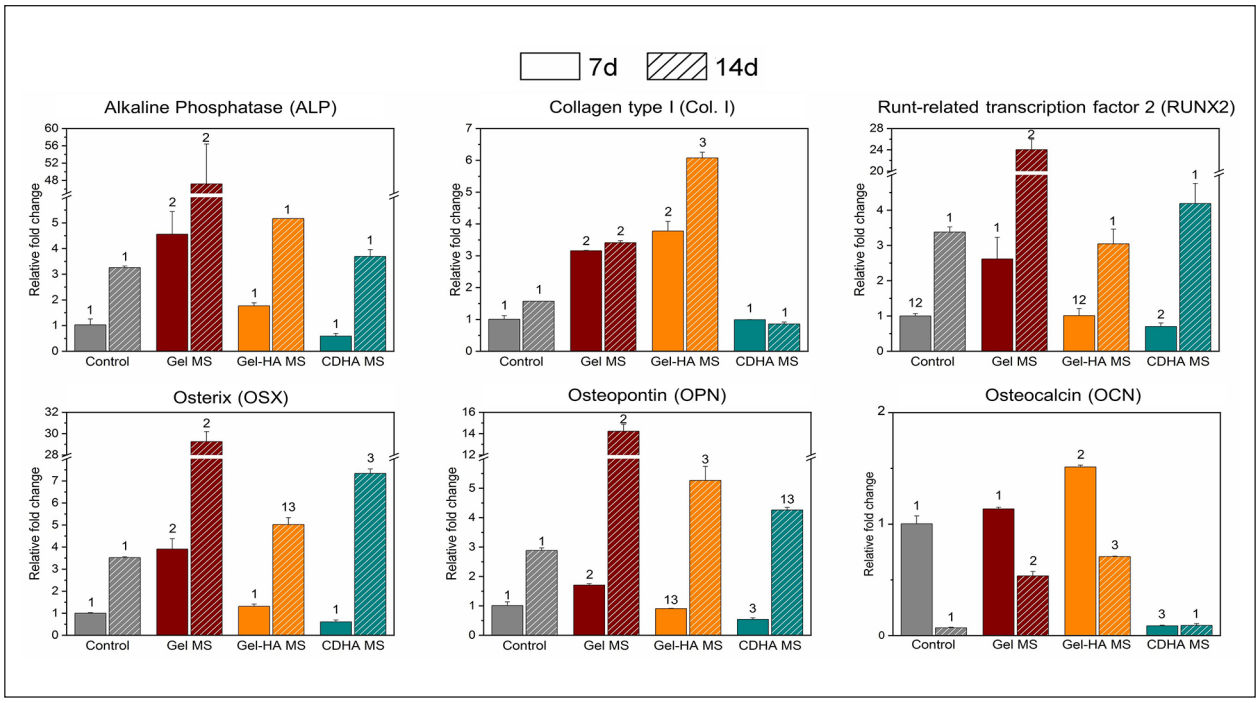

Figure 6. Gene expression of osteogenic markers for the cells in wCL bioinks at day 7 and 14 of culture. Control bioink at day 7 was used as a reference to determine the fold changes. Different numbers indicate statistically significant differences between conditions at each time point ($p < 0.05$).

incorporation of microspheres increased both the G'_{eq} and the yield stress that are directly related to the extrudability and shape fidelity of the bioinks. Indeed, the incorporation of fillers in hydrogels is a common strategy to improve their mechanical properties, where the resulting composite partially exhibits the mechanical features of their individual components. When a load is applied to these materials, it will be transferred from the polymer to the stiffer filler (in our case, the cross-linked Gel MS and the mineral-containing MS), which will bear part of the load, increasing the global mechanical properties.[45] We observed that the extent of these changes highly depended on the nature of each MS. Precisely, Gel MS doubled the G'_{eq} compared to the control, Gel-HA MS presented a $>$ 10-fold increase, while for CDHA MS only a limited gain was observed. Regarding the yield stress, in Gel MS and CDHA MS remained similar to the control, while in Gel-HA MS it was 3 times higher (Table 2). These differences can be attributed to the marked volume gain of the Gel-HA MS in aqueous media compared to the other types of MS (Figure 1(b)), that generated a higher MS/alginate ratio for the same initial volume. Moreover, the apatite-containing MS might present higher rigidity than the Gel MS, which may contribute to the final rheological properties of the hydrogels. Although one could hypothesise that, since these MS contain Ca^{2+}, this ion could be released and contribute to the cross-linking of the alginate, we consider this phenomenon as highly improbable for two reasons. First, as shown in the ICP-OES results (Figure 1(e)), no Ca^{2+} release was recorded in DMEM, which is the medium where the alginate was dissolved to prepare the inks. Secondly, no effect was found in this sense with the CDHA MS, that also contain Ca^{2+}.

Regarding the 3-ITT results (Figure 2(b)), a fast and almost complete elastic recovery was registered for all the conditions. This is generally linked to the shape fidelity of the filaments and is fundamental in the future development of 3D-printed structures, together with a proper self-supporting capacity.[44]

Apart from controlling the shape fidelity during the extrusion, it was crucial to ensure sufficient mechanical stability of the bioprinted ink when immersed in cell culture medium. This was explored investigating two different cross-linking protocols for the alginate hydrogel, which consisted in varying the initial $CaCl_2$ bath time and the supplementation or not of the cell culture media throughout the study (i.e. wCL consisting of 10 min CL in 150 mM $CaCl_2$, and sCL consisting of 15 min CL with 150 mM $CaCl_2$ and additional supplementation of up to 5 mM $CaCl_2$ in the cell culture medium during the culture). Increasing the CL from 10 to 15 min did not have any substantial effect. The initial G′ value for both CL conditions was ≈10,000 Pa, comparable to the results of cross-linked hydrogels previously reported in the literature.[46–48] This parameter, which accounts for the stiffness of the bioink and is related to the self-supporting capacity of the extruded and cross-linked filaments, did not change

between the two CL (Figure 2(c)). In contrast, the Ca^{2+} supplementation in the culture media was crucial for the bioink stability during the subsequent days of incubation. Indeed, rheology results displayed important differences in the loss of G′ between the two CL conditions at both day 7 and 14, with variations of up to 40% in the Gel-HA MS samples at day 14 (Figure 2(d)). The loss of stiffness is associated with the hydrogel degradation, which can be explained by the exchange of divalent by monovalent cations that revert the gelation of alginate, destabilising the hydrogel network and solubilising the polymer.[49,50] For this reason, the addition of $CaCl_2$ to the culture media permitted better stability in sCL bioinks compared to wCL ones, allowing to study the cell performance up to 21 days of culture instead of the 14 days of the wCL conditions.

In order to investigate the performance of the synthesised MS, viability, proliferation and cell morphology studies were performed with MG-63 cells seeded directly onto the MS. In addition, the expression of several osteoblastic differentiation genes was explored. MG-63 cells, which have an immature pre-osteoblastic phenotype, were used for cell culture studies. As an immortalised cell line, they are an unlimited cell source and have a more reliable reproducibility than primary cells.[51] The large number of conditions that were tested *in vitro*, together with the high cell concentration these studies required, urged us to work with reliable and fast-growing cells. The results summarised in Figure 3 demonstrated that MG-63 cells were able to attach and grow on the MS, showing a good proliferation rate in all the tested conditions. They presented a similar morphology among conditions. Regarding gene expression, CDHA MS showed, overall, higher levels of all osteogenic genes at all the time points. Hence, it can be stated that CDHA MS had better osteoinductive properties than the other MS. The high capacity of certain calcium phosphate materials to induce osteogenic differentiation of stem cells has been largely described,[31,41] mostly related to the triggered ion exchange and specific morphological features such as their porosity, geometry and specific surface area. Despite Gel-HA MS also upregulated certain genes compared to the control sample, no major differences were observed between Gel MS and Gel-HA MS.

A step forward in this investigation was to assess the behaviour of MG-63 cells embedded in bioinks containing the synthesised MS. Prior to the cell culture, two cross-linkings were performed, a weak and a strong cross-link to assess not only the mechanical stability of the constructs but also the capacity of the cells to migrate to the MS and proliferate. The first aspect explored was the effect of shear stress during the extrusion on cell viability. The results showed that the dispensation through the nozzle was one of the most critical steps for the cells in 3D-bioprinted inks. In fact, during extrusion-based bioprinting cells are exposed to different mechanical forces, where shear stress is the main cause of cell death.[52] Gel-HA MS and CDHA MS bioinks presented a statistically significant reduction of 20% in the cell survival rate (Figure 4(c)), revealing that the incorporation of ceramic-based MS was unfavourable for the cells at the extrusion step. Notwithstanding, it was the rheology of Gel-HA MS bioink which clearly differed from the other conditions, presenting flow stress of ≈3000 Pa compared to the other formulations where it was near 1000 Pa (Table 2). Since in the Gel MS condition the survival rate of the cells was high, it indicates that the shear forces applied cannot be the reason for the cell death in the bioinks with mineral-loaded MS. In fact, similar shear stress values have been reported to present high cell survival.[53] From this point of view, it is not clear the cause of the initial cell death and further investigation would be required. Despite the slight reduction in cell viability for some of the conditions during extrusion, the subsequent cell culture up to 21 days showed similar proliferation behaviour regardless of the MS type.

Notwithstanding, the results revealed that the rigidity of the alginate hydrogel extremely influenced cell behaviour. First, the L/D images exhibited substantial differences in cell migration between the two CL conditions, as MG-63 started attaching to the MS mainly at day 3 in the wCL bioinks while for sCL samples cell attachment to the MS was delayed starting at day 7 (Figure 4(a)). Moreover, proliferation data in Figure 5(a) also supported the impact of bioink stiffness on the cells: in the wCL MS-containing bioinks cells were able to proliferate to a great extent at day 3, whereas in the sCL this phenomenon did not happen until day 14. Therefore, the results demonstrated the need of viscosity relaxation for the cells to migrate, attach and proliferate inside the bioinks. These findings are in agreement with previous literature, where several works proved that the stiffness of the bioink directly affects the cell performance at different extents. For instance, it has been reported that softer matrices seem to promote hMSC spreading,[54] proliferation[48] and their differentiation to a neurogenic lineage, while stiffer hydrogels tend to induce osteogenesis.[55] In conclusion, the cross-linking conditions of hydrogels is a fundamental issue in bioink development and must be optimised to have the desirable cell behaviour without compromising the mechanical stability of the construct.

Cells embedded in the different bioinks presented spherical morphologies, and only when attached to the MS were able to spread (Figure 4(a)). In addition, MG-63 presented a highly proliferative profile in all the samples, rising up to 4-fold the initial cell number in wCL bioinks (Figure 5(b)). Nonetheless, the system forced the cells to proliferate on themselves forming cell clusters, where the cells remained spherical. Cell proliferation in alginate hydrogels has been extensively studied in the literature, and controversial results have been published. Indeed, several studies report that cells are not able to proliferate due to the lack of cell adhesive sites in the alginate molecule,

which usually leads to hydrogel modification by the incorporation of high amounts of RGD peptides.[56,57] In contrast, other studies showed that alginate by itself supports cell proliferation, although exhibiting rounded-shaped cells.[50] The same phenomenon has been observed in other hydrogels with cell-adhesive moieties, where it is thought that their highly hydrophilic microenvironment force the cells to spherical shapes.[58] The capacity of the cells to easily spread is a crucial point, as some 3D microenvironments can prevent osteogenic differentiation by restricting cell growth and cell spreading.[59] Therefore, the presence of particles that serve as cell attaching points is one of the strengths of the present approach, as it allows the normal phenotype and function of the cells.

Regarding the gene expression of the cells embedded in the bioinks, RT-qPCR results indicated that the highest expression of certain osteogenic genes such as ALP, RUNX2, OSX and OPN occurred in Gel MS bioinks, with significant differences compared to the other types of MS (Figure 6). These findings differ from the results obtained in the cells seeded directly onto the MS, where CDHA MS were found to be the ones that better promote the osteogenic differentiation (Figure 3(d)). It is important to highlight that in the case of the cell-laden inks, not only the contribution of the cells attached to the MS was analysed, but also the gene expression of the cells forming spheroids within the alginate. Therefore, the most feasible explanation is that the marked cell differentiation in Gel MS bioink compared to the other conditions was due to the direct contact of the cells with the MS, which was shown to be substantially higher in this condition than in the other specimens. In fact, apart from the physicochemical properties of the material, cell-material interaction has been reported to have a significant influence in cell differentiation.[60,61] The reason why the cells were not able to colonise the CDHA MS could be their limited swelling in wet conditions compared to the rest of the MS (Figure 1(b)). This reduced swelling behaviour creates a less packed MS network in the bioink that forces the cells to move farther to reach the MS. In view of the differences in the osteogenic markers' expression between the bioinks and the direct cell seeding onto the MS, it was demonstrated that changes in the system and, thus, in cell environment largely influenced cell behaviour. The ability of the cells to move inside the hydrogel and migrate to reach the MS proved that pre-seeding of the cells in the MS prior to their incorporation into the bioink was not needed. However, the attachment to the CDHA MS was not shown to be effective, which hindered their osteogenic properties, and a pre-seeding would be a strategy to boost it. Therefore, pre-seeded MS can be used to assure cell attachment and incorporated into the bioink after 1–3 days in culture, depending on the MS nature and the cell type studied.

The present strategy, based on the incorporation of microspheres in cell-laden inks, offers promising perspectives. First, the versatility of the approach enables its extrapolation to fields other than bone regeneration. For instance, using MS of other natures and even as drug-release or ion release agents, may allow to transfer this solution into other applications such as chondral regeneration, soft tissue or ocular tissue engineering. Moreover, the system provides a versatile soft matrix for more complex biofabrication approaches. For example, it can be combined with core/shell strategies localising the MS either in the shell or the core of the strands to confer them specific functionalities.[62] Finally, as the proposed solution is simple and robust, it would open the path to become a product more accessible than other more sophisticated cell therapies found in the literature.

Conclusion

The introduction of microspheres of different natures (i.e. gelatine, gelatine containing hydroxyapatite nanoparticles and CDHA) into an alginate-based bioink allowed not only to tune its rheological properties but also to modulate the cell performance. While direct cell seeding of MG-63 cells on the different MS proved the superior osteogenic potential of the fully mineral MS, gene expression of the cells embedded in the bioinks indicated higher expression on the Gel MS bioinks consistent with a superior migration capacity of cells on these MS. Moreover, the migration ability was clearly affected by the size of the MS and the stiffness of the bioink, which could be adjusted by the cross-linking time. Overall, this work proves the potential of using MS as a simple tool to adjust bioink functionality.

Acknowledgements

M-P. Ginebra acknowledges the Generalitat de Catalunya for the ICREA Academia Award and M. Espanol for the Serra Hunter Program. Experimental assistance of Elisabetta Gioffrè is highly appreciated.

Declaration of conflicting interests

The author(s) declared no potential conflicts of interest with respect to the research, authorship, and/or publication of this article.

Funding

The author(s) disclosed receipt of the following financial support for the research, authorship, and/or publication of this article: This work was supported by the Spanish Ministry of Science, Innovation and Universities through the project PID2019-103892RB-I00/AEI/10.13039/501100011033; M.Bonany acknowledges the Spanish Government for the Ph.D. grant BES-2016-07672; M-P. Ginebra acknowledges the Generalitat de Catalunya for funding through the ICREA Academia Award.

ORCID iD

Montserrat Espanol https://orcid.org/0000-0001-7510-0602

Supplemental material

Supplemental material for this article is available online.

References

1. Abbott A. Cell culture: biology's new dimension. *Nature* 2003; 424: 870–872.
2. Andersen T, Auk-Emblem P and Dornish M. 3D cell culture in alginate hydrogels. *Microarrays* 2015; 4: 133–161.
3. Do AV, Khorsand B, Geary SM, et al. 3D printing of scaffolds for tissue regeneration applications. *Adv Healthc Mater* 2015; 4: 1742–1762.
4. Levato R, Jungst T, Scheuring RG, et al. From shape to function: the next step in bioprinting. *Adv Mater* 2020; 32: e1906423.
5. Malda J, Visser J, Melchels FP, et al. 25th anniversary article: engineering hydrogels for biofabrication. *Adv Mater* 2013; 25: 5011–5028.
6. Murphy SV and Atala A. 3D bioprinting of tissues and organs. *Nat Biotechnol* 2014; 32: 773–785.
7. Gungor-Ozkerim PS, Inci I, Zhang YS, et al. Bioinks for 3D bioprinting: an overview. *Biomater Sci* 2018; 6: 915–946.
8. Matai I, Kaur G, Seyedsalehi A, et al. Progress in 3D bioprinting technology for tissue/organ regenerative engineering. *Biomaterials* 2020; 226: 119536.
9. Hernández-González AC, Téllez-Jurado L and Rodríguez-Lorenzo LM. Alginate hydrogels for bone tissue engineering, from injectables to bioprinting: A review. *Carbohydr Polym* 2020; 229: 115514.
10. Piras CC and Smith DK. Multicomponent polysaccharide alginate-based bioinks. *J Mater Chem B* 2020; 8: 8171–8188.
11. Li Z, Huang S, Liu Y, et al. Tuning alginate-gelatin bioink properties by varying solvent and their impact on stem cell behavior. *Sci Rep* 2018; 8(1): 8020.
12. Jia J, Richards DJ, Pollard S, et al. Engineering alginate as bioink for bioprinting. *Acta Biomater* 2014; 10: 4323–4331.
13. Sarker MD, Naghieh S, McInnes AD, et al. Bio-fabrication of peptide-modified alginate scaffolds: printability, mechanical stability and neurite outgrowth assessments. *Bioprinting* 2019; 14: e00045.
14. Ning L, Zhu N, Mohabatpour F, et al. Bioprinting Schwann cell-laden scaffolds from low-viscosity hydrogel compositions. *J Mater Chem B* 2019; 7: 4538–4551.
15. Rowley JA, Madlambayan G and Mooney DJ. Alginate hydrogels as synthetic extracellular matrix materials. *Biomaterials* 1999; 20: 45–53.
16. Dhoot NO, Tobias CA, Fischer I, et al. Peptide-modified alginate surfaces as a growth permissive substrate for neurite outgrowth. *J Biomed Mater Res* 2004; 71A: 191–200.
17. Heid S and Boccaccini AR. Advancing bioinks for 3D bioprinting using reactive fillers: a review. *Acta Biomater* 2020; 113: 1–22.
18. Ojansivu M, Rashad A, Ahlinder A, et al. Wood-based nanocellulose and bioactive glass modified gelatin-alginate bioinks for 3D bioprinting of bone cells. *Biofabrication* 2019; 11: 035010.
19. Olmos Buitrago J, Perez RA, El-Fiqi A, et al. Core-shell fibrous stem cell carriers incorporating osteogenic nanoparticulate cues for bone tissue engineering. *Acta Biomater* 2015; 28: 183–192.
20. Demirtaş TT, Irmak G and Gümüşderelioğlu M. A bioprintable form of chitosan hydrogel for bone tissue engineering. *Biofabrication* 2017; 9: 035003.
21. Lin H-R and Yeh Y-J. Porous alginate/hydroxyapatite composite scaffolds for bone tissue engineering: preparation, characterization, andin vitro studies. *J Biomed Mater Res* 2004; 71B: 52–65.
22. Luo Y, Lode A, Wu C, et al. Alginate/nanohydroxyapatite scaffolds with designed core/shell structures fabricated by 3D plotting and in situ mineralization for bone tissue engineering. *ACS Appl Mater Interfaces* 2015; 7: 6541–6549.
23. Levato R, Visser J, Planell JA, et al. Biofabrication of tissue constructs by 3D bioprinting of cell-laden microcarriers. *Biofabrication* 2014; 6: 035020.
24. Tan YJ, Tan X, Yeong WY, et al. Hybrid microscaffold-based 3D bioprinting of multi-cellular constructs with high compressive strength: a new biofabrication strategy. *Sci Rep* 2016; 6(1): 39140.
25. Abu Awwad HAM, Thiagarajan L, Kanczler JM, et al. Genetically-programmed, mesenchymal stromal cell-laden & mechanically strong 3D bioprinted scaffolds for bone repair. *J Control Release* 2020; 325: 335–346.
26. Wang P, Meng X, Wang R, et al. Biomaterial scaffolds made of chemically cross-linked gelatin microsphere aggregates (C-GMSs) promote vascularized bone regeneration. *Adv Healthc Mater* 2022; 11: e2102818.
27. Bednarzig V, Schrüfer S, Schneider TC, et al. Improved 3D printing and cell biology characterization of inorganic-filler containing alginate-based composites for bone regeneration: particle shape and effective surface area are the dominant factors for printing performance. *Int J Mol Sci* 2022; 23: 4750.
28. Xu M, Liu T, Qin M, et al. Bone-like hydroxyapatite anchored on alginate microspheres for bone regeneration. *Carbohydr Polym* 2022; 287: 119330.
29. Zhao Z, Espanol M, Guillem-Marti J, et al. Ion-doping as a strategy to modulate hydroxyapatite nanoparticle internalization. *Nanoscale* 2016; 8: 1595–1607.
30. Perez RA, Del Valle S, Altankov G, et al. Porous hydroxyapatite and gelatin/hydroxyapatite microspheres obtained by calcium phosphate cement emulsion. *J Biomed Mater Res Part B Appl Biomater* 2011; 97: 156–166.
31. Barba A, Diez-Escudero A, Maazouz Y, et al. Osteoinduction by foamed and 3D-printed calcium phosphate scaffolds: effect of nanostructure and pore architecture. *ACS Appl Mater Interfaces* 2017; 9: 41722–41736.
32. Schindelin J, Arganda-Carreras I, Frise E, et al. Fiji: an open-source platform for biological-image analysis. *Nat Methods* 2012; 9: 676–682.
33. Muyonga JH, Cole CG and Duodu KG. Fourier transform infrared (FTIR) spectroscopic study of acid soluble collagen and gelatin from skins and bones of young and adult Nile perch (Lates niloticus). *Food Chem* 2004; 86: 325–332.
34. Berzina-Cimdina L and Borodajenko N. Research of calcium phosphates using Fourier transform infrared spectroscopy. In: Theophanides T (ed.) *Infrared spectroscopy – Materials science, engineering and technology*. London: IntechOpen, 2012, pp.123–148.
35. Koutsopoulos S. Synthesis and characterization of hydroxyapatite crystals: A review study on the analytical methods. *J Biomed Mater Res* 2002; 62: 600–612.

36. Diez-Escudero A, Espanol M, Beats S, et al. In vitro degradation of calcium phosphates: effect of multiscale porosity, textural properties and composition. *Acta Biomater* 2017; 60: 81–92.
37. Fleet ME. The carbonate ion in hydroxyapatite: recent X-ray and infrared results. *Front Biosci* 2013; 5: 643–652.
38. Rey C, Marsan O, Combes C, et al. Characterization of calcium phosphates using vibrational spectroscopies. In: Ben-Nissan B(ed.) *Advances in calcium phosphate biomaterials. Springer series in biomaterials science and engineering*. Berlin, Heidelberg: Springer, 2014, Vol. 2, pp. 229–266.
39. Wang X, Ao Q, Tian X, et al. Gelatin-based hydrogels for organ 3D bioprinting. *Polymers* 2017; 9: 401.
40. Dorozhkin SV. Nanosized and nanocrystalline calcium orthophosphates. *Acta Biomater* 2010; 6: 715–734.
41. Barradas A, Yuan H, van Blitterswijk C, et al. Osteoinductive biomaterials: current knowledge of properties, experimental models and biological mechanisms. *Eur Cell Mater* 2011; 21: 407–429.
42. Xing Q, Yates K, Vogt C, et al. Increasing mechanical strength of gelatin hydrogels by divalent metal ion removal. *Sci Rep* 2014; 4: 4706.
43. Gustavsson J, Ginebra MP, Engel E, et al. Ion reactivity of calcium-deficient hydroxyapatite in standard cell culture media. *Acta Biomater* 2011; 7: 4242–4252.
44. Schwab A, Levato R, D'Este M, et al. Printability and shape fidelity of bioinks in 3D bioprinting. *Chem Rev* 2020; 120: 11028–11055.
45. Ji D and Kim J. Recent strategies for strengthening and stiffening tough hydrogels. *Adv NanoBiomed Res* 2021; 1: 2100026.
46. Lueckgen A, Garske DS, Ellinghaus A, et al. Enzymatically-degradable alginate hydrogels promote cell spreading and in vivo tissue infiltration. *Biomaterials* 2019; 217: 119294.
47. Lueckgen A, Garske DS, Ellinghaus A, et al. Hydrolytically-degradable click-crosslinked alginate hydrogels. *Biomaterials* 2018; 181: 189–198.
48. Wei Q, Young J, Holle A, et al. Soft Hydrogels for balancing cell proliferation and differentiation. *ACS Biomater Sci Eng* 2020; 6: 4687–4701.
49. Bajpai SK and Sharma S. Investigation of swelling/degradation behaviour of alginate beads crosslinked with $Ca2^{+}$ and Ba2+ ions. *React Funct Polym* 2004; 59: 129–140.
50. Grigore A, Sarker B, Fabry B, et al. Behavior of ncapsulated MG-63 cells in RGD and gelatine-modified alginate hydrogels. *Tissue Eng Part A* 2014; 20: 2140–2150.
51. Czekanska EM, Stoddart MJ, Richards RG, et al. In search of an osteoblast cell model for in vitro research. *Eur Cell Mater* 2012; 24: 1–17.
52. Boularaoui S, Al Hussein G, Khan KA, et al. An overview of extrusion-based bioprinting with a focus on induced shear stress and its effect on cell viability. *Bioprinting* 2020; 20: e00093.
53. Nair K, Gandhi M, Khalil S, et al. Characterization of cell viability during bioprinting processes. *Biotechnol J* 2009; 4: 1168–1177.
54. Duarte Campos DF, Blaeser A, Buellesbach K, et al. Bioprinting organotypic hydrogels with improved mesenchymal stem cell remodeling and mineralization properties for bone tissue engineering. *Adv Healthc Mater* 2016; 5: 1336–1345.
55. Engler AJ, Sen S, Sweeney HL, et al. Matrix elasticity directs stem cell lineage specification. *Cell* 2006; 126: 677–689.
56. Hafeez S, Ooi HW, Morgan FLC, et al. Viscoelastic oxidized alginates with reversible imine type crosslinks: Self-Healing, injectable, and Bioprintable Hydrogels. *Gels* 2018; 4: 85.
57. Fonseca KB, Bidarra SJ, Oliveira MJ, et al. Molecularly designed alginate hydrogels susceptible to local proteolysis as three-dimensional cellular microenvironments. *Acta Biomater* 2011; 7: 1674–1682.
58. Wang C, Gong Y, Zhong Y, et al. The control of anchorage-dependent cell behavior within a hydrogel/microcarrier system in an osteogenic model. *Biomaterials* 2009; 30: 2259–2269.
59. Major LG, Holle AW, Young JL, et al. Volume adaptation controls stem cell mechanotransduction. *ACS Appl Mater Interfaces* 2019; 11: 45520–45530.
60. Rychly J and Nebe BJ. Cell-material interaction. *BioNanoMaterials* 2013; 14: 153–160.
61. Hanson S, D'Souza RN and Hematti P. Biomaterial-mesenchymal stem cell constructs for immunomodulation in composite tissue engineering. *Tissue Eng Part A* 2014; 20: 2162–2168.
62. Akkineni AR, Ahlfeld T, Lode A, et al. A versatile method for combining different biopolymers in a core/shell fashion by 3D plotting to achieve mechanically robust constructs. *Biofabrication* 2016; 8: 045001.